A FINITE ELEMENT METHOD FOR SHEAR STRESSES CALCULATION IN COMPOSITE BLADE MODELS

B. Paluch

Institut de Mécanique des Fluides de Lille
IMFL - ONERA
5, Boulevard Paul Painlevé
59000 Lille - France

Notations

C^i_{kl}	Shear elastic constants of the materials
E_i	Young's modulus of the material of the phase β_i, in the x direction
n_y, n_z	components of a unit normal vector located on a free edge of the section
g_0	transverse shear warping function
k_z	reduced section coefficient
u', v', w'	components of the warping displacement induced by the torsion
u'', v'', w''	components of the warping displacement induced by shearing and normal forces
β_i	phase, *i.e.* a material making up a distinct part of a blade section
η	warping at a point P of a section, induced by shearing and normal forces
Φ	warping function of torsion associated to the center of torsion C
ϕ	warping function of torsion associated to the elastic center E
Θ	unit angle of torsion of the section
$\theta_x, \theta_y, \theta_z$	rigid body angles of rotation of the section about the X,Y, and Z axes
Ω	rotational speed of the blade
γ_s, γ_r	shear strains
σ_s, σ_r	shear stresses

Abstract

When dimensioning helicopter blade models, it is important to be able to calculate the shear stresses induced by torsion and shearing forces in each section accurately. The method explained here can be used to compute these stresses once the two warping functions are determined that represent the torsional and transverse shear properties of the blade. The finite element formulations associated with these functions are formally identical, except as concerns the boundary conditions. This method can also be used to compute the equivalent torsional stiffness of the sections, their transverse shear coefficients, and the position of their center of torsion. A grid generator method is also discussed, which is a part of the calculation program, and is used to discretize the sections quickly and condition the grid data reliably. After describing the successful validation of the method on a few sections composed of isotropic materials, we apply it to the case of blade model sections made of composite materials. The results are good, compared with experimental data.

Introduction

Aeroelastic computation algorithms are of capital importance in the design of helicopter blade models for use in wind tunnel tests. If theese blades are made of composite materials, their globa· elastic characteristics can then be adapted more easely to their operating mode, by creating structurai couplings that will reduce the level of vibration at the rotor head, for example, and increase the flight performances. However, one of the major steps during the dimensioning process consists in verifying the mechanical strength of the blades under the effect of the loads they will be sustaining in the wind tunnel.

That is, these blades must be able to stand up to the very heavy loads of testing for long enough to avoid any risk of breakage, which would disrupt the process and spoil the results. Contrary to the normal stresses on the blades, which can be calculated easely by conventional materials strength theory, the shear stresses generated in the blade sections for certain loading configurations may become predominant and thereby decrease the nominal lifetime. However, in spite of all the advantages that militate in favor of composite materials for these models, one disadvantage resides in the fact that it is no longer possible to compute the shear stress distributions on the blade sections by simple analytical methods. To remedy this, the method proposed here is based on a finite element determination of two warping functions, representative of the torsional and transverse shear properties, from which the shear stresses are computed. As the blade structures are relatively complex, a grid generator program is needed to discretize the sections. We will be describing the principle of operation of this generator.

Equivalent Elastic Characteristics of the Sections

A local frame of reference is attached to each blade section (figure 1) with the x axis located at the fore quarter chord of the airfoil (generally the same as the pitch axis), the y axis is identified with the chord of the airfoil and directed from leading to trailing edge, and the z axis is right-hand orthonormal to the other two axes. The blade is driven in uniform rotational motion Ω.

As a helicopter blade is composed of N different materials, we call each of the material making up a distinct part of the section a phase β_i (i=1,N) and then define the following centers :

- E   the elastic center of the section;
- C   the center of torsion of the section;
- G   the center of gravity of the section;
- O   the intersection of the pitch axis with the section plane.

The position of the elastic center E is defined as the barycenter of the Young's moduli E_i along the x axis of each phase, weighted by the areas S_i that they occupey. The position of the elastic center in the (O,x,y,z) frame of reference is computed from the equivalent tensile stiffness <ES> anᶜ from the following barycentric formulae :

$$y_E = \frac{1}{<ES>} \sum_{i=1}^{N} E_i \iint_{S_i} y \, dS$$

<div align="right">(1-1)</div>

$$z_E = \frac{1}{<ES>} \sum_{i=1}^{N} E_i \iint_{S_i} z \, dS$$

<div align="right">(1-2)</div>

In the same frame (E,x,y,z) of reference, we can compute the equivalent stiffnesses in flapping mode $<EI_{yy}>$, lead-lag $<EI_{zz}>$, and flap-lead-lag coupling $<EI_{yz}>$. The angle of inclination α of the main inertial reference frame system (E,X,Y,Z) with respect to (E,x,y,z) is found by diagonalizing the following inertia matrix :

$$\begin{pmatrix} <EI_{yy}>-\lambda & <EI_{yz}> \\ <EI_{yz}> & <EI_{zz}>-\lambda \end{pmatrix} = 1$$

<div align="right">(2)</div>

The eigenvalues λ_1 and λ_2 are equal to the main flapping and lead-lag stiffnesses $<EI_{YY}>$ and $<EI_{ZZ}>$. Lastly, still in the main inertial frame of reference, we define the equivalent transverse shear stiffnesses $<GS_Y>$ and $<GS_Z>$. The mathematical definitions of these quantities are given in appendix A. These equivalent elastic characteristics, which are extensive quantities, are easely calculated by classical integration methods like the Gauss method [1]. However, as we will see further on, the equivalent torsional stiffness $<GJ>$ cannot be calculated by simple methods in the case of sections made of composite materials. This is possible only for simply or multiply connected sections like box-structures, made up of an isotropic material. The warping function ϕ of the section has to be determined in order to find the value of $<GJ>$.

In the following we will consider the blades to be solids having beam type properties, *i.e.* as structures having a sufficiently large aspect ratio (span-to-chord). To remain within the bounds of beam-type theory, this aspect ratio generally has to be greater than or equal to ten.

<u>Forces, moments and displacements</u>

For a section located at a distance r from the center of rotation of the rotor, the force tensor applied to this section reduces to the following six components (figure 2) :

- N_x the tensile force normal to the section;
- T_y, T_z the shearing forces acting in the flapping and lead-lag planes;
- M_x the moment of torsion;
- M_y, M_z the flapping and lead-lag moments.

In the main axis system (E,X,Y,Z) and according to elasticity theory as applied to straight and curved beams, the normal strain ε_{xx} of an arbitrary point P in the section has the value :

$$\varepsilon_{xx} = \varepsilon_{xx}^{0} + yR_z + zR_y$$

(3)

ε_0 being the elongation due to the normal force, R_y and R_z being the local curvatures induced by the moments M_y and M_z. These quantities are deduced from the following system of equations :

$$\begin{pmatrix} <ES> & 0 & 0 \\ 0 & <EI_{ZZ}> & 0 \\ 0 & 0 & <EI_{YY}> \end{pmatrix} \begin{pmatrix} \varepsilon_0 \\ R_Z \\ R_Y \end{pmatrix} = \begin{pmatrix} N_X \\ -M_Z \\ M_Y \end{pmatrix}$$

(4)

as long as the sections remain flat after deformation, either by a displacement parallel to themselves along the x axis, or rigid rotations θ_y and θ_z about the Y and Z axes at O. In this case, the only nonzero stress is the normal stress σ_{xx} such that :

$$\sigma_{xx} = E_i \, \varepsilon_{xx} = E_i \, (\frac{N_x}{<ES>} - y \, \frac{M_z}{<EI_{ZZ}>} + z \, \frac{M_y}{<EI_{YY}>})$$

(5)

Of course, such a constitutive equation cannot be used to work back to the shear stresses. In modern blades, the introduction of composite materials with their shear moduli and their failure stresses much below those of metallic materials (or foam cores whose shear characteristics are even weaker than those of composite materials), special attention must be paid to the problem of the shear strength of composite materials. Similarly, in certain cases the transverse shear effects on th vibratory properties of the blades have to be taken into account [2] [3] [4].

Under the effect of the torsion and transverse shear, the sections will be warped, and for a point P located in a given section, the components displacement field (u,v,w) is expressed as a function of the sum of two independant displacement fields, which are :

- the displacements u',v',w' due to the warping of the section by torsion;
- the displacements u'',v'',w'' due to the warping of the section under the effect of the transverse shear.

Thus :

$$u = u' + u'' \;,\; v = v' + v'' \;,\; w = w' + w''$$

(6)

in which :

$$u' = \Theta\phi(y,z) \;,\; v' = - \Theta xz \;,\; w' = \Theta xy$$

(7)

where ϕ is the Saint-Venant warping function expressed in the main inertial frame of reference, and Θ the unit angle of rotation of the section about the x axis such that $\Theta = d\theta_x/dx$. The displacements v' and w' being the rigid body motion of the section. And :

$$u'' = u_0 - y\theta_z + z\theta_y + \eta_{xx}(y,z) + \eta_{xy}(y,z) + \eta_{xz}(y,z) \;,\; v'' \sim 0 \;,\; w'' \sim 0$$

(8)

in which η_{xy}, η_{xz} and η_{xx} are the x-wise warp displacements due to the shearing forces T_y and T_z, and the normal force N_x (figure 3). The warping function Φ that normally has to be determined with respect to the torsion center (x,y,z) at C can also be calculated in the main inertial frame of reference, with respect to which it is denoted ϕ, by the variable conversion :

$$\Phi(y,z) = \phi(Y,Z) - yz_C + zy_C$$

$$(9)$$

in which (y_C, z_C) are the coordinates of the center of torsion in the (x,y,z) frame of reference at O. As the position of the center of torsion is not known beforehand, ϕ can be determined because it is proven that the determination of the Saint-Venant warping function is, with an appropriate variable conversion, independent of the frame of reference chosen, because the equation governing it contains only terms including second-order derivatives.

By integrating, over one section, the equations of equilibrium of elasticity, expressed in the absence of body forces, or :

$$\sigma_{ij,j} = 0 \quad i,j = x,y,z$$

$$(10)$$

This brings us back to the classical beam theory equations relating the forces and moments to the blade loading conditions, with :

$$\frac{\partial N_x}{\partial x} + q_x = 0 \ , \ q_x = m_1 \Omega^2 x$$

$$(11)$$

in the X direction, m_1 being the mass per unit length of the blade for a section located at a spanwise abscissa x ,

$$\frac{\partial T_y}{\partial x} + q_y = 0 \ , \ \frac{\partial M_z}{\partial x} + T_y = 0$$

$$(12\text{-}1)$$

$$\frac{\partial T_z}{\partial x} + q_z = 0 \ , \ \frac{\partial M_y}{\partial x} + T_z = 0$$

$$(12\text{-}2)$$

q_y and q_z being the distributions per unit length of the shearing forces exerted in the Y and Z planes of the blade, assuming that the moments per unit length are zero and that the effects of the finite point forces are negligible compared with that of the loadings per unit length.

Stresses and Strains

The stress tensor at a point P of the section is expressed :

$$\overline{\overline{\sigma}}(P) = \begin{pmatrix} \sigma_{xx} & \sigma_{xy} & \sigma_{xz} \\ \sigma_{yx} & \sigma_{yy} & \sigma_{yz} \\ \sigma_{zx} & \sigma_{zy} & \sigma_{zz} \end{pmatrix}$$

$$(13)$$

The resultant x-wise stress $\vec{T}(P,x)$ at point P therefore has the value :

$$\vec{T}(P,x) = \bar{\bar{\sigma}}.\vec{n}$$

(14)

with the components σ_{xx}, σ_{xy}, and σ_{xz}.

As the lateral surfaces of the sections are under very little load, because of the low value of the aerodynamic pressure field exerted on the airfoil, the stresses in the Y-Z (E) plane are then considered to be zero, or :

$$\sigma_{yy} = \sigma_{yz} = \sigma_{zz} = 0$$

(15)

However, although the effect of the pressure field is intrinsically negligible, it must be taken into account in the form of a loading per unit length, having two components q_y and q_z. The forces of inertia set up by the flapping and lead-lag oscillations of the blade also reduce to two loadings per unit length that are superimposed on those of the aerodynamic pressure field. Finally, following hypothesis (15) adopted above, the stress tensor is written :

$$\bar{\bar{\sigma}}(P) = \begin{pmatrix} \sigma_{xx} & \sigma_{xy} & \sigma_{xz} \\ \sigma_{yx} & 0 & 0 \\ \sigma_{zx} & 0 & 0 \end{pmatrix}$$

(16)

We have seen that, in the main inertial frame of reference, the normal stress σ_{xx} has a simple expression when the section warp is not taken into account. When it is, the strain ε_{xx} has the value :

$$\varepsilon_{xx} = \frac{\partial u''}{\partial x} = \frac{\partial u_0}{\partial x} - y\frac{\partial \theta_z}{\partial x} + z\frac{\partial \theta_y}{\partial x} + \frac{\partial}{\partial x}(\eta_{xx} + \eta_{xy} + \eta_{xz})$$

(17)

Yet the variation in the warp between two infinitely contiguous sections may be considered negligible, so that :

$$\frac{\partial}{\partial x}(\eta_{xx} + \eta_{xy} + \eta_{xz}) = 0 \; , \; \frac{\partial \phi}{\partial x} = 0$$

(18)

which for the strain ε_{xx}, finally yields an expression identical to (3).

Still following the principle of superimposition, the shear stress field will be equal to the sum of the two stress fields, with :

$$\sigma_{xy} = \sigma'_{xy} + \sigma''_{xy}$$ (19-1)

$$\sigma_{xz} = \sigma'_{xz} + \sigma''_{xz}$$ (19-2)

in which the primes and double primes denote, respectively, the contributions of the torsion and of the transverse shear. Returning to the first of the equilibrium equations of (10), or :

$$\frac{\partial \sigma_{xx}}{\partial x} + \frac{\partial \sigma_{xy}}{\partial y} + \frac{\partial \sigma_{xz}}{\partial z} = 0$$

(20)

we get :

$$\frac{\partial \sigma'_{xy}}{\partial y} + \frac{\partial \sigma'_{xz}}{\partial z} = 0$$

<div align="right">(21-1)</div>

$$\frac{\partial \sigma''_{xy}}{\partial y} + \frac{\partial \sigma''_{xz}}{\partial z} = E_i \left(-\frac{\partial N_x}{\partial x} \frac{1}{<ES>} + y \frac{T_y}{<EI_{ZZ}>} - z \frac{T_z}{<EI_{YY}>} \right)$$

<div align="right">(21-2)</div>

We will now use the following example to show that two of the terms of equation (21-2) can be neglected. In the case of a blade model used for wind tunnel testing, let us take the following realistic values :

$<ES> = 4.10^2$ N , $<EI_{YY}> = 1600$ N.m^2 , $<EI_{ZZ}> = 35000$ N.m^2 , $m_l = 2$ kg.m^{-1}

$x = 2$ m , $\Omega = 100$ rd.s^{-1} , $T_y = T_z = 1000$ N

After calculation, the contributions of the terms on the right-hand side of (21-2) are arranged in increasing order as follows :

$$\frac{\partial N_x}{\partial x} \frac{1}{<ES>} \# 10^{-3} \ll \frac{T_y}{<EI_{ZZ}>} = 3.10^{-2} < \frac{T_z}{<EI_{YY}>} = 0.6$$

In other words, the first two terms of (21-2) have values that are about 600 times and 20 times less, respectively, than the contribution of the third term alone, depending on the shearing force Tz . This makes the contribution of these first two terms negligible compared to the third. Moreover, since the flapping stiffness $<EI_{YY}>$ is still very much less than the lead-lag stiffness $<EI_{ZZ}>$, it is clear that the system of equations (21), may, after simplification, be reasonably written :

$$\frac{\partial \sigma'_{xy}}{\partial y} + \frac{\partial \sigma'_{xz}}{\partial z} = 0$$

<div align="right">(22-1)</div>

$$\frac{\partial \sigma''_{xy}}{\partial y} + \frac{\partial \sigma''_{xz}}{\partial z} = -z \frac{E_i T_z}{<EI_{YY}>}$$

<div align="right">(22-2)</div>

It is this system of equations which we can now use to compute the warping functions. However, to simplify the writing of the equations governing these functions, we will adopt an abbreviated subscript notation that is commonly used in composite material structural calculations, expressing the double subscripts with a single one as follows :

xx -> x , xy -> s , xz -> r

so that the stresses become :

σ_{xx} -> σ_x , σ_{xy} -> σ_s , σ_{xz} -> σ_r

Using this notation, we express the stress-strain relation for a phase β_i of given anisotropic behavior in the matrix form :

$$\begin{pmatrix} \sigma_s \\ \sigma_r \end{pmatrix} = \begin{pmatrix} C^i_{ss} & C^i_{sr} \\ C^i_{sr} & C^i_{rr} \end{pmatrix} \begin{pmatrix} \gamma_s \\ \gamma_r \end{pmatrix}$$

<div align="right">(23)</div>

with :

$$\gamma_s = \gamma'_s + \gamma''_s$$

$$\gamma_r = \gamma'_r + \gamma''_r$$

(24)

and the C^i_{kl} representing the shear mode elastic constants of the material.

For the torsion contribution, we have :

$$\gamma'_s = \frac{\partial u'}{\partial y} + \frac{\partial v'}{\partial x} = \Theta \left(\frac{\partial \Phi}{\partial y} - (z - z_C) \right) = \Theta \left(\frac{\partial \phi}{\partial y} - z \right)$$

(25-1)

$$\gamma'_r = \frac{\partial u'}{\partial z} + \frac{\partial w'}{\partial x} = \Theta \left(\frac{\partial \Phi}{\partial y} + (y - y_C) \right) = \Theta \left(\frac{\partial \phi}{\partial z} + y \right)$$

(25-2)

While the transverse shear contribution is expressed by :

$$\gamma''_s = - \theta_z + \frac{\partial \eta_{xz}}{\partial y} \quad , \quad \gamma''_r = \theta_y + \frac{\partial \eta_{xz}}{\partial z}$$

(26)

Détermination of the Warping Functions

Torsion

When equation (22-1) is extended to matrix form it becomes :

$$\left(\frac{\partial}{\partial y} , \frac{\partial}{\partial z} \right) \left(\begin{array}{cc} C^i_{ss} & C^i_{sr} \\ C^i_{sr} & C^i_{rr} \end{array} \right) \left(\begin{array}{c} \frac{\partial \phi}{\partial y} - z \\ \frac{\partial \phi}{\partial z} + y \end{array} \right) = 0$$

(27)

or, taking the products :

$$C^i_{ss} \frac{\partial^2 \phi}{\partial y^2} + C^i_{rr} \frac{\partial^2 \phi}{\partial z^2} + 2 C^i_{sr} \frac{\partial^2 \phi}{\partial y \partial z} = 0$$

(28)

The boundary condition is a free edge condition, *i.e.* the resultant stress vector at any point of the free surface ∂S, expressed in the X direction tangential to this free lateral surface, leads to the following matrix equation :

$$(n_y , n_z) \left(\begin{array}{cc} C^i_{ss} & C^i_{sr} \\ C^i_{sr} & C^i_{rr} \end{array} \right) \left(\begin{array}{c} \frac{\partial \phi}{\partial y} \\ \frac{\partial \phi}{\partial z} \end{array} \right) = (n_y , n_z) \left(\begin{array}{cc} C^i_{ss} & C^i_{sr} \\ C^i_{sr} & C^i_{rr} \end{array} \right) \left(\begin{array}{c} z \\ -y \end{array} \right)$$

(29)

Another boundary condition, and one which is implicitly built into this system of equations, sets the resultants stress vectors equal on either side of the boundary between two phases β_i and β_j. This assumes that there is a perfect adherence between two contiguous phases.

We see that the general problem of the torsion of the straight sections consisting of isotropic or anisotropic materials is expressed using an equation of partial derivatives (27) coupled to an equation (29) expressing the free edge boundary condition. The value of the equivalent torsional stiffness $<GJ>$ is deduced from the torsion moment M_x, since :

$$<GJ> = \frac{M_x}{\Theta} = \frac{1}{\Theta} \int\int_{S_i} (y\, \sigma_r - z\, \sigma_s)\, dS$$

(30)

which, by substituting their values for σ_r and σ_s, yields :

$$<GJ> = \int\int_{S_i} \{ \frac{\partial f}{\partial y} (yC_{sr}^i - zC_{ss}^i) + \frac{\partial f}{\partial z} (yC_{rr}^i - zC_{sr}^i) + (z^2 C_{ss}^i + y^2 C_{rr}^i - 2yz C_{sr}^i) \} dS$$

(31)

Finally, the Principle of Virtual Works [5] [6] is used to compute the position (y_c, z_c) of the center of torsion, with :

$$y_c = - \frac{1}{<EI_{YY}>} \sum_{i=1}^{N} E_i \int\int_{S_i} z\, \phi\, dS$$

(32-1)

$$z_c = \frac{1}{<EI_{ZZ}>} \sum_{i=1}^{N} E_i \int\int_{S_i} y\, \phi\, dS$$

(32-2)

Tranverse Shear

When equation (22-2) is expanded for the transverse shear, as was done for the torsion, a matrix form similar to that of equation (27) is obtained that is :

$$\left(\frac{\partial}{\partial y}, \frac{\partial}{\partial z} \right) \begin{pmatrix} C_{ss}^i & C_{sr}^i \\ C_{sr}^i & C_{rr}^i \end{pmatrix} \begin{pmatrix} \frac{\partial \eta_{xz}}{\partial y} - \theta_z \\ \frac{\partial \eta_{xz}}{\partial z} + \theta_y \end{pmatrix} = - \frac{z\, E_i\, T_z}{<EI_{YY}>}$$

(33)

In its contracted form, this equation becomes :

$$C_{ss}^i \frac{\partial^2 \eta_{xz}}{\partial y^2} + C_{rr}^i \frac{\partial^2 \eta_{xz}}{\partial z^2} + 2\, C_{sr}^i \frac{\partial^2 \eta_{xz}}{\partial y \partial z} = - \frac{z\, E_i\, T_z}{<EI_{YY}>}$$

(34)

Nevertheless, by a variable conversion such that :

$$\eta_{xz} = \frac{T_z}{<GS_z>} \, g(y,z)$$

(35)

equation (34) is expressed in terms of the warping functions g rather than the displacement η_{xz}, or :

$$C_{ss}^i \frac{\partial^2 g}{\partial y^2} + C_{rr}^i \frac{\partial^2 g}{\partial z^2} + 2 \, C_{sr}^i \frac{\partial^2 g}{\partial y \partial z} = - z \, E_i \frac{<GS_z>}{<EI_{YY}>}$$

(36)

Here again, the boundary condition is a free edge condition, since the resultant stresses vector must be zero. This yields :

$$(\, n_y \, , \, n_z \,) \begin{pmatrix} C_{ss}^i & C_{sr}^i \\ C_{sr}^i & C_{rr}^i \end{pmatrix} \begin{pmatrix} \frac{\partial g}{\partial y} \\ \frac{\partial g}{\partial z} \end{pmatrix} = \frac{<GS_z>}{T_z} (n_y \, , \, n_z \,) \begin{pmatrix} C_{ss}^i & C_{sr}^i \\ C_{sr}^i & C_{rr}^i \end{pmatrix} \begin{pmatrix} \theta_z \\ -\theta_y \end{pmatrix}$$

(37)

At this stage, a simplification can still be introduced at the level of (37) since, as we have seen, the flapping stiffness is very much less than the lead-lag stiffness. This implies that the angle of rotation θ_z of the section is negligible compared with the angle of rotation θ_y, as a consequence of expression (37), which after simplification becomes :

$$(\, n_y \, , \, n_z \,) \begin{pmatrix} C_{ss}^i & C_{sr}^i \\ C_{sr}^i & C_{rr}^i \end{pmatrix} \begin{pmatrix} \frac{\partial g}{\partial y} \\ \frac{\partial g}{\partial z} \end{pmatrix} = \frac{<GS_z>}{T_z} \theta_y \, (n_y \, , \, n_z \,) \begin{pmatrix} C_{ss}^i \\ C_{sr}^i \end{pmatrix}$$

(38)

Moreover, a second variable conversion such that :

$$g = g_0 - k_z \, z$$

(39)

gives us a rational way of introducing the reduced section coefficient k_z such that :

$$k_z = \frac{<GS_z>}{T_z} \theta_y$$

(40)

in which g_0 represents the warping function, and which is calculated from the relation :

$$k_z = \frac{1}{<EI_{YY}>} \sum_{i=1}^{N} E_i \iint_{S_i} g_0 \, z \, dS$$

(41)

Proceeding with the variable conversion defined in (39) in expression (38), by identification we find again the value of k_z given in (40), which means that the boundary condition is very simply formulated by taking :

$$(n_y , n_z) \begin{pmatrix} C^i_{ss} & C^i_{sr} \\ C^i_{sr} & C^i_{rr} \end{pmatrix} \begin{pmatrix} \dfrac{\partial g_0}{\partial y} \\ \dfrac{\partial g_0}{\partial z} \end{pmatrix} = 0$$

(42)

The continuity condition between two contiguous phases β_i et β_j on g_0 is implicitely verified, as it was for the torsion.

Finite Element Formulation

In the integral formulation of the finite element problem, equations (28) and (29) are expressed symbolically in the form .
$$L(\phi) = 0 \ , \ C(\phi) = f_s$$

(43)

Similarly, for equations (34) and (42), we have :
$$L(g_0) = f_v \ , \ C(g_0) = 0$$

(44)

In both cases, the operators $L(*)$ and $C(*)$ are identical with :
$$L(*) = (\frac{\partial^2(*)}{\partial y^2} C^i_{ss} + 2 \frac{\partial^2(*)}{\partial y \partial z} C^i_{sr} + \frac{\partial^2(*)}{\partial z^2} C^i_{rr})$$

(45-1)

$$C(*) = (\frac{\partial(*)}{\partial y} (n_y C^i_{ss} + n_z C^i_{sr}) + \frac{\partial(*)}{\partial z} (n_y C^i_{sr} + n_z C^i_{rr}))$$

(45-2)

At this stage it is interesting to note that, on a formal level, the solutions to the torsion and transverse shear problems are identical, except as far as the boundary conditions are concerned. In the torsion case, the body forces are zero while the boundary condition requires equivalent surface forces. For the transverse shear, the surface forces are zero, resulting in a body force equal to the second member of equation (36).

The finite element problem is solved in the usual way, by discretizing the sections with a certain number of elements, at the nodes of which the two nodal unknowns ϕ et g_0 , representative of the warp, are computed. After putting together the equivalent stiffness and force matrices, the following two linear systems are solved simultaneously :
$$[K'] \{ \phi \} = \{ F' \}$$

(46-1)

$$[K''] \{ g_0 \} = \{ F'' \}$$

(46-2)

in which { F'} represents the surface forces that have to be intoduced in order to include the boundary conditions expressed in (29), and { F" } the body forces deriving from the second member of (26). Though these body forces would be easy to calculate, the blade section grid generator program has to be able to index the free edges of the elements in order to be able to

calculate $\{ F' \}$. This grid generator program also has to determine the composite material fiber orientation angles in each of the phases β_i , so that the base change on the elastic constants C^i_{ss}, C^i_{rr} and C^i_{sr} , when each element is calculated.

Although the simplest elements to use are isoparametric elements with three-node triangular linear interpolation (T3) and four-node rectangular elements (Q4), we chose rather to use quadratic interpolation elements with six and eight nodes (T6-Q8), because we wanted to get a good approximation of the shear stress field with a reasonable number of elements, which leads to much better precision in the final result because the stresses are calculated from the warping function derivatives. What is more, the precision of the results is isensitive to any geometric distorsions of the elements during the grid generation procedure, contrary to what happens for elements with linear interpolation [6].

Determining the Elastic Constants for the Materials Making up the Sections

For an arbitrary phase β_i of anisotropic material, the elastic constants C^i are in principle random because the local frame of reference and the orthotropic axes of the material are not the same. For isotropic and transverse isotropic materials, the elastic constants remain invariable, while for orthotropic materials they depend on the direction of the reinforcement (figure 4). Generally speaking, two possible cases may exist in the blade sections :

- either a composite with unidirectional reinforcement, in which case the fibers lie in the plane of the section at an arbitrary angle of inclination δ with respect to the main axes o inertia (figure 4b);

- or a laminated blade consisting of a stack of several layers of unidirectional or woven reinforcement, in which case the equivalent shear elastic constants have to be computed using laminate theory (figure 4c).

In both cases, the matrix of elastic constants obey the base change formula :

$$\begin{pmatrix} C^i_{ss} & C^i_{sr} \\ C^i_{sr} & C^i_{rr} \end{pmatrix} = \begin{pmatrix} m & -n \\ n & m \end{pmatrix} \begin{pmatrix} C^i_{44} & 0 \\ 0 & C^i_{55} \end{pmatrix} \begin{pmatrix} m & n \\ -n & m \end{pmatrix}$$

(47)

in which m=cos(δ), n=sin(δ) , while C^i_{44} and C^i_{55} are the planar and transverse shear stiffnesses expressed in the orthotropic frame of reference of the phase β_i .

Meshing of the Blade Sections

The structure of the blades, considering their geometry and the internal arrangement of materials, is sufficiently complex to justify the use of a specific grid generator program. The method we used consists in partitioning the section into sub-domains, with the mesh characteristics (number an distribution of elements) stipulated inside each one. To make sure the mesh remains continuous

from one subdomain to the next, the only condition that has to be fulfilled is to have identical node distributions on the edges of each contiguous pair of subdomains. The subdomains may have three sides (ten-node Lagrange type interpolation) or four (twelve-node Serendip type interpolation), so that there is a great deal of flexibility for partitioning any type of section (figure 5). In both cases, the subdomain edges are defined by four interpolation points, so that any edges there may be that have double curvature can still be modeled.

In the skin layers of the section, for example, the plies have a local orietation that follows the curvature of the aerodynamic profile. Since two of the edges follow this profile (the thickness of the ply remaining constant), by computing the local orientation at the subdomain definition nodes, we can interpolate to find the local orientation of any node located within this subdomain (figure 6).

The subdomain definition node coordinates are not entered directly in the grid generator because this would be long and fastidious. Moreover, the position of these nodes would have to be determined by some other means, such as a CAD tool. The approach we adopted rather consists in smoothing the aerodynamic profile with cubic splines, then discretizing with a certain number of dedimensionalized definition points (*i.e.* points normalized with respect to the airfoil chord), and finally computing for each (figure 6a) :
- the abscisses and ordinates on the airfoil upper and lower surfaces;
- the director coefficients of the inward normals on the upper and lower surfaces (figure 6b).

The director coefficients of these normals are used to calculate the position of the lower part of the skin of the section by removing the total thickness of the layers it contains, and after having placed the airfoil at the chord (figure 6c). Since the skin of a given section may include plies of different thicknesses with an arbitrary chordwise distribution, the composition of the skin is described be entering, for each slice :
- its position;
- the composition of the skin (number of layers, types of materials, etc ....).

The skin thicknesses and the elastic characteristics of the composites making it up, are automatically computed from the thicknesses and elastic characteristics of each layer. In the same way, the inside of the blade is divided into several sections that may each be made up of several layers, distributed thicknesswise. The thickness of each layer may vary, as may the type of material. Figure 7 gives three examples of how the internal distribution of material can be described. Figure 8 shows an example of a blade section partitioned into subdomains, including a trailing edge spar, a foam core and a leading edge spar, as well as the final grid. The foam core was not meshed because, due to its very low mechanical strength characteristics, its contribution to the overall stiffness of the section is quite negligible. The normals at the free edges of the section are also shown in this figure. These are used for computing the surface forces that have to be applied in order to comply with the free-edge boundary conditions (equation 29, figure 8c), as well as the tangents at each node of the elements corresponding to the skin, which are used for computing base changes of the elastic constants (equation 47, figure 8d).

Once the double nodes are eliminated, there is a subroutine that finishes by renumbering the nodes to minimize the necessary memory space. This is done by the method of constructing global stiffness matrices in a skyline, which considerably reduces the necessary computation time. When renumbering this way, the nodes are projected onto an axis that is slightly inclined with respect to the airfoil chord, and are then renumbered in increasing order of appearance as one travels along this line from leading to trailing edge. Figures 8e and 8f show the memory maps of the global stiffness matrices before and after renumbering.

Results and Discussion

Sections of Isotropic Material

We started by comparing the results of our computation method with those of known exact analytical solutions for the two section geometries - rectangular and tubular - consisting of a steel-type material with isotropic properties (shear modulus G=84.6 GPa).

For the rectangular section (figure 9a), the analytical formulation is given by the solution of the problem of isotropic beam torsion using Prandtl stress function Ψ [7], such that :

$\Delta \Psi = -2$ in the domain (D) of the section;

$\Psi = 0$ on its contour (∂S);

$$(48)$$

which, after solving the system of equations (48), yields :

$$\Psi(y,z) = \frac{32\,b^2}{\pi^3} \sum_{n=0}^{\infty} \frac{(-1)^n}{(2n+1)^3} \left(1 - \frac{ch\lambda_n y}{ch\lambda_n a} \right) cos\lambda_n z \qquad , \qquad \lambda_n = \frac{(2n+1)}{2b}\,\pi$$

$$(49)$$

and :

$$\sigma'_{xy} = G\,\Theta\,\frac{\partial \Psi}{\partial z} \quad , \quad \sigma'_{xz} = G\,\Theta\,\frac{\partial \Psi}{\partial y} \quad , \quad <GJ> = 2\,G \int_{-a}^{a} \int_{-b}^{b} \Psi\,dy\,dz$$

$$(50)$$

The warping function Φ is related to the function Ψ by the relation :

$$\Psi = \Phi - \frac{1}{2}\,(y^2 + z^2)$$

$$(51)$$

Because the section is symmetrical, its center of torsion C is the same as its center of symmetry O. Consequently, the warping function g_0 can be found from the relation :

$$\nabla^2 g_0 = -z\,\frac{E}{G}\,\frac{<GS_z>}{<EI_{YY}>} = -12\,\frac{z}{h^2}$$

$$(52)$$

which yields :

$$g_0 = \frac{3}{2} z - 2 \frac{z^3}{h^2}$$

<div align="right">(53)</div>

and :

$$\sigma''_{xy} = 0 \quad , \quad \sigma''_{xz} = \frac{T}{<GS_z>} G \frac{dg_0}{dz} = \frac{T}{8ab} (\frac{3}{2} - 6 \frac{z^2}{h^2}) \quad , \quad k_z = \frac{6}{5}$$

<div align="right">(54)</div>

Let us note that, in the case of isotropic rectangular sections, the shear stress distibution can be found using the Timoshenko function [7]. The mesh adopted for the computation includes 36 Q8 elements. The difference between the <GJ> calculated analytically (equation 50, <GJ>= 9.91 10⁴ N.m²) and the one found by the finite element computation is less than 0.14 %. The same is true for the value of the reduced section coefficient k_z, which is less than 0.7 %.

Figures 9b and 9c show the variations of the warping and shear stress functions for the torsion and transverse shear calculated for $\Theta = 2°/m$ and $T_z = 10^5$ N. We observe that the differences between the theoretical curves and the values obtained by finite element remain small even in areas of high stress or torsion gradients. The warping displacements (u' and u" components) of the sections are visualized in figures 9d and 9e. In this simple case, we see that, despite the low number of elements used, the degree of precision of the finite element method is already excellent.

Because of its geometry, the second section is already closer to helicopter blade type sections. This is a symmetrical, doubly connex simple airfoil (figure 10a) for which the torsional stiffness is determined analytically using the membrane analogy method [8], with :

$$<GJ> = 4 G e \frac{S_\Gamma^2}{L_\Gamma}$$

<div align="right">(55)</div>

in which e is the airfoil thickness, L_Γ the perimeter of the mean curve Γ and S_Γ the surface it encompasses. The mesh of the section includes 14 elements and the difference between the <GJ> does not exceed 1.2 % (<GJ>=1.084 10³ N.m² for the computation with (55)). The resultant shear stresses τ such that :

$$\tau = \sqrt{\sigma'^2_{xy} + \sigma'^2_{xz}} = <GJ> \frac{\Theta}{2 e S_\Gamma}$$

<div align="right">(56)</div>

were calculated at each of the element integration points. The stress predicted by the membrane theory is assumed to be constant in the airfoil wall, since this wall is thin compared with the largest dimensions of the airfoil. The differences between the computed and theoretical resultant stresses, given in figure 10b, are less than 1%. The transverse shear effect was not computed for this section because we were more interested in doing this for sandwich-type rectangular sections were the core has a large effect on the coefficient of the reduced section.

Sandwich-Structures Sections

There is no longer any need to demonstrate the effect of transverse shear in the computation of sandwich structures [2] [3] [4], chiefly as concerns their natural frequencies. To show that the finite element method yields correct values for the k_z coefficient, three types of rectangular sandwich sections were studied. Their external dimensions (80 mm wide for a total thickness of 30 mm) were all identical, but their total thickness to skin thickness ratios differed from 3 to 6 to 15.

The grids for these sections, which can be seen in figure 11, include between 36 and 48 elements. The skins of aluminum alloy have a Young's modulus E_p of 74.6 GPa, and the core consists of a material that can be likened to foam, with a Young's modulus ten, 100 or 1,000 times less than that of the skins, for each of the sections studied. The analytical formula for calculating the theoretical k_z can be found in [3]. The theoretical and computed values of k_z are given in the following table along with the differences :

(ep+ea)/ep ->	3			6			15		
Ep/Ea	Kz th.	Kz cal.	Dif. %	Kz th.	Kz cal.	Dif. %	Kz th.	Kz cal.	Dif. %
1 0	4.89	4.89	0.	3.89	3.89	0.	2.26	2.26	0.
1 0 0	43.3	43.3	0.	31.9	31.9	0.	14.1	14.1	0.
1 0 0 0	4 2 7	4 1 7	2.3	3 1 2	3 0 3	2.9	1 3 3	1 3 0	2.3

For Young's modulus ratios of up to 100, the differences are null; but they still do not exceed 3% when this ratio is 1,000. As in the case of torsion, just a small number of elements yields very good results. Although we currently have no method for measuring k_z, the agreement between theoretical and experimental results for transverse shear is excellent in these simple configurations. Moreover, the sandwich plates are close to helicopter blades in structure, with their foam or honeycomb cores. This method therefore hold promise for applications to helicopter blades.

Blade Model Sections

We have seen above that, for simple sections of an isotropic materials, it was possible to compare the results of a computation with exact analytical solutions, or approximate solutions given by classical elasticity theory, for purposes of validation. For blade sections, on the other hand, there is no precise, nor even approximate, computation method. The only quantity that can be easely measured experimentally is the equivalent torsional stiffness <GJ>, and we will assume in the current state of affairs that the estimation of the warping field ϕ of a blade section is better, the closer the computed values of <GJ> are those measured.

In the case of transverse shear, we do not have a sufficiently precise experimental method for measuring the coefficient k_z at the current time, which would reasonably allow us to adopt the same assumption as for torsion. However, on the basis of the study previously made for sandwich sections, we may consider that, from a prediction point of view, the finite element method yield good results as far as the determination of the shear stresses induced by the shearing forces is concerned.

<GJ> is measured by clamping a blade section at one of its ends and subjecting the other end to a torsional torque (figure 12). Two mirrors (or more) are fastened on this section a distance l apart, far enough away from the points where the blade is clamped and where the torque is applied. The position of the luminous points from the beams, reflected off these mirrors and measured on a frosted glass located at a distance L from the blade section, is used to compute the angle of rotation between two contiguous sections, by :

$$\Theta_x = \Delta / 2L$$

since $\Delta \ll L$. Each value of the torsional torque M_x^k applied to the section corresponds to an angle of torsion Θ_x^k. The regression line passing through the n pairs (k=1,n) of points (M_x^k, Θ_x^k) yield the value of <GJ> while minimizing the effect of the measurement uncertainties.

The first two sections studied have identical geometries but consist of different materials. They are derived from rigid blades manufactured by the IMFL for research on helicopter rotor stability [9]. These two blade sections have a NACA 0016 section and a chord of 50 mm, and are made of (figure 8a) :

-    a skin of constant thickness;
-    leading and trailing edge spars of unidirectional composite with fibers lying spanwise;
-    a core of low-density polyurethane foam.

The grid (figure 8b) includes 87 elements and no foam core, whose mechanical contibution is null. The first section (the "glass" blade) was a composite made of E glass fiber and epoxy resin. The characteristics are given in the following table :

Component	Material	Ex (GPa)	Gs (GPa)	Gr (GPa)
Spars	UD GlassE/epoxy	43	4.2	4.2
Skin	Satin8 woven GlassE/epoxy	21	5.1	2.5

The following table lists the equivalent mechanical characteristics for the materials used to make the second section ("graphite" blade) :

Component	Material	Ex (GPa)	Gs (GPa)	Gr (GPa)
Spars	UD HS Graphite/ep	148	5.1	5.1
Skin	Laminate HM Graphite/ep [(+/-45°)]	213	65	2.9

The calculated and measured values of the <GJ> , of the k_z coefficients, as well as the positions of the elastic and torsional centers of these two sections, are given in the following table :

	"Glass" blade	"Graphite" blade
<GJ> measured [N.m2]	10.88	72.7
<GJ> calculated [N.m2]	10.14	68.4
Diference [%]	6.8	5.9
Kz	7.14	1.78
Elastic center [chord %]	29.6	21.4
Torsion center [chord %]	26.8	20.2

The differences between the <GJ> values, though greater than those found in the case of isotropic sections, are small. They may nonetheless be partly explained by the fact that there exists some uncertainty in the <GJ> measurement, and because the elastic characteristics of the composite materials are generally slightly dispersive. The coefficient k_z is greater in the case of the "glass" blade because of the low Young's modulus of the skin material for this section. The warping displacements in torsion and transverse shear are visualized in figures 13a and 13b for the "glass" blade. It can be seen in the case of torsion that the warp is greater with increased distance from the center of torsion and is at its maximum at the level of the trailing edge, because of the small thickness of the airfoil at this point. Similarly, the constant-stress maps are given in figures 13c and 13d, where it can be seen that it is the skin that takes the bulk of the shear stresses.

The last blade section studied (figure 14a) consists of :
-    a skin of laminated material having one ply of E glass/epoxy, and a series of plies of unidirectional HR graphite/epoxy, oriented at +45° and -45°, arranged in decreasing thickness from the leading edge to the trailing edge;
-    two unidirectional R glass/epoxy spars;
-    a foam core;
-    a tube of light alloy embedded in the foam core.

The tube of light alloy and the foam core were not included in the grid (figure 11b). The computed and measured values are listed together in the following table :

<GJ> measured	<GJ> calculated	Difference	Elastic center	Torsion center
1392 N.m2	1510 N.m2	8.5 %	24.3 % chord	35.4 % chord

The difference between the <GJ> values is equivalent to that obtained for the previously computed sections, for the same reasons as we have already mentionned. The computed constant-stress maps for a unit angle of torsion $\Theta=5$ °/m are plotted in figures 14c and 14d. These stresses, which are predominant at the level of the skin, are practically null in the spars. Let us note that the complexity of the leading edge spar does little to change the stress distributions from what they are in figure 13. That is, for the same level of stress, the spar is deformed more than the skin because of the low shear modulus of the unidirectional composite it is made of.

Conclusion

The program that was developped and applied to various sections of isotropic and composite materials can be used to compute the shear stresses induced by torsion and shear forces. It yields good results as concerns the prediction of equivalent torsion stiffness, and shear stresses induced by torsion. The computation of the reduced-section coefficient and of the shear stresses induced by th shearing forces also yields good results as concerns the isotropic sections, compared to the stresses

calculated by analytical solutions. There is no particular problem extending it to blade sections of composite materials; but a method will be needed in the near future to measure the reduced-section computations directly or indirectly on blade model sections. It would, for example, be possible to start with an identification method using vibratory analysis systems. However, to be complete, the validation of the method as a whole will have to be continued on other blade models, and the shear stresses will have to be measured and compared to those calculated by the finite element method.

The grid generation method we propose, for its part, discretizes the blade sections quickly and reliably. Moreover, it automatically computes the additional data needed, both to comply with the boundary conditions specific to the torsion problem, and also to include the special characteristics related to the types of materials the blades are made of.

Lastly, let us point out that in addition to the determination of the warping functions, it will now be possible to compute the global coupling terms, in bending-torsion, for example, that are indispensable to other algorithms currently being developped [10] [11] [12].

Références

[1] B. Paluch, Calculation of equivalent elastic characteristics and fatigue life of helicopter blade model sections (in French), **I.M.F.L. Report**, N° 91/18, August 1991

[2] D. Gay, M. Carrier, J.M. Cieaux, J.J. Barrau, Influence du cisaillement transversal sur les vibrations de flexion des structures sandwiches, **ECCM1 First European Conference on Composite Materials**, Bordeaux (France) , 24 - 27th Sept. 1985 , pp. 114-119

[3] S. Vlachoutsis, S. Laroze, Shear correction factors for multilayered plates and shells, **Composites-Structures** , A. Niku-Lari Editor, I.I.T.T. Institut Industriel de Transfert de Technologie, Nice (France), 20-22th June 1988, pp. 125-138

[4] A. Fages , G. Verchery, Transverse shear influence on calculus of natural frequencies of sandwich beams, **Proceedings of the 3rd International Conference on Composite Structures**, I.H. Marshall Editor , Elsevier , Paisley (U.K.), 1985, Vol. 3 , pp. 643-659

[5] D. Gay, Matériaux composites, Hermès, 1987

[6] J.J. Barrau, O. Chambard, D. Gay, M. Nuc, Evaluation of torsion characteristics for a composite beam (in French), **Proceedings of the 3rd congress on structure calculation**, Pluralis, Bastia (France), 6-8th Nov 1985, pp. 284-296

[7] L. Solomon, Elasticité linéaire, Masson, 1968

[8] Timoshenko, Résistance des matériaux, Masson, Tome 2, 1968

[9] J.J. Costes, I. Cafarelli, N. Tourjansky, Theoretical and experimental study of a rotor model, **16th European Rotorcraft Forum**, Glasgow (U.K.), 18-20th sept. 1990, Paper N°III-9-2, 14 p.

[10] A. Laulusa, Theoretical and experimental investigation of the large deflection of beams, American Helicopter Society, **International Meeting on Rotorcraft Basic Research**, Georgia Institute of Technology, Atlanta (U.S.A.), March 1991, Paper N°14, 19 p.

[11] P. Minguet, J. Dugundji, Experiments and analysis for composite blades under large deflection Part I : static behavior, **AIAA Journal**, Vol.28, N°9, Sept.1990, pp. 1573-1579

[12] P. Minguet, J. Dugundji, Experiments and analysis for composite blades under large deflection Part II : dynamic behavior, **AIAA Journal**, Vol.28, N°9, Sept.1990, pp. 1580-1588

APPENDIX A

$$<ES> = \sum_{i=1}^{N} E_i S_i$$

$$<EI_{yy}> = \sum_{i=1}^{N} E_i \iint_{S_i} z^2 dS$$

$$<EI_{zz}> = \sum_{i=1}^{N} E_i \iint_{S_i} y^2 dS$$

$$<EI_{yz}> = \sum_{i=1}^{N} E_i \iint_{S_i} yz dS$$

$$<GS_y> = \sum_{i=1}^{N} G_{xy}^i S_i$$

$$<GS_z> = \sum_{i=1}^{N} G_{xz}^i S_i$$
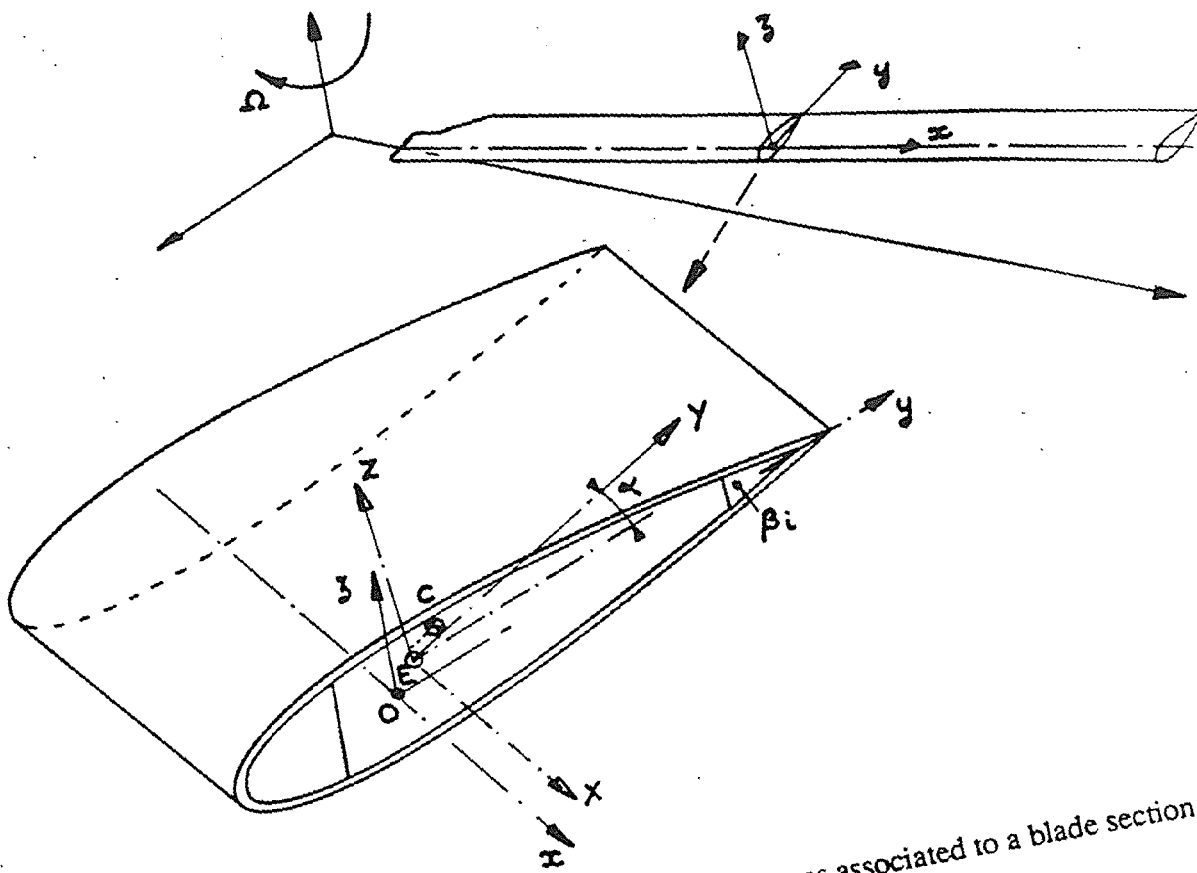
Figure 1 :   Definition of the axes systems associated to a blade section
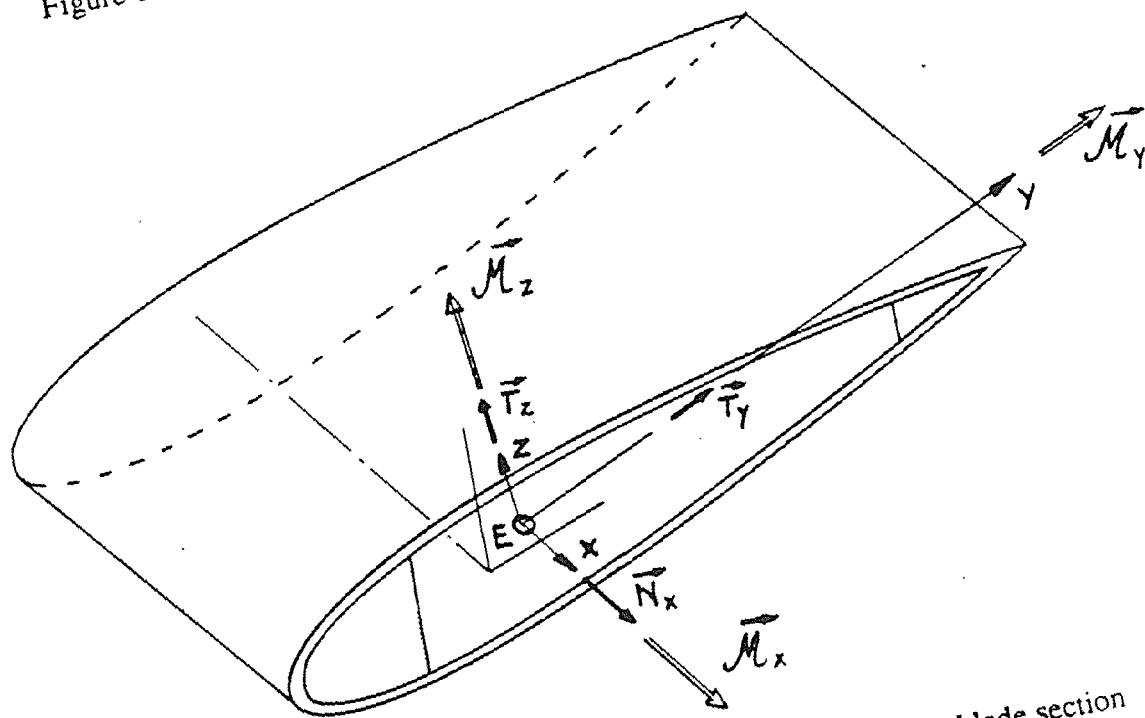
Figure 2 :   Forces and moments components acting on a blade section
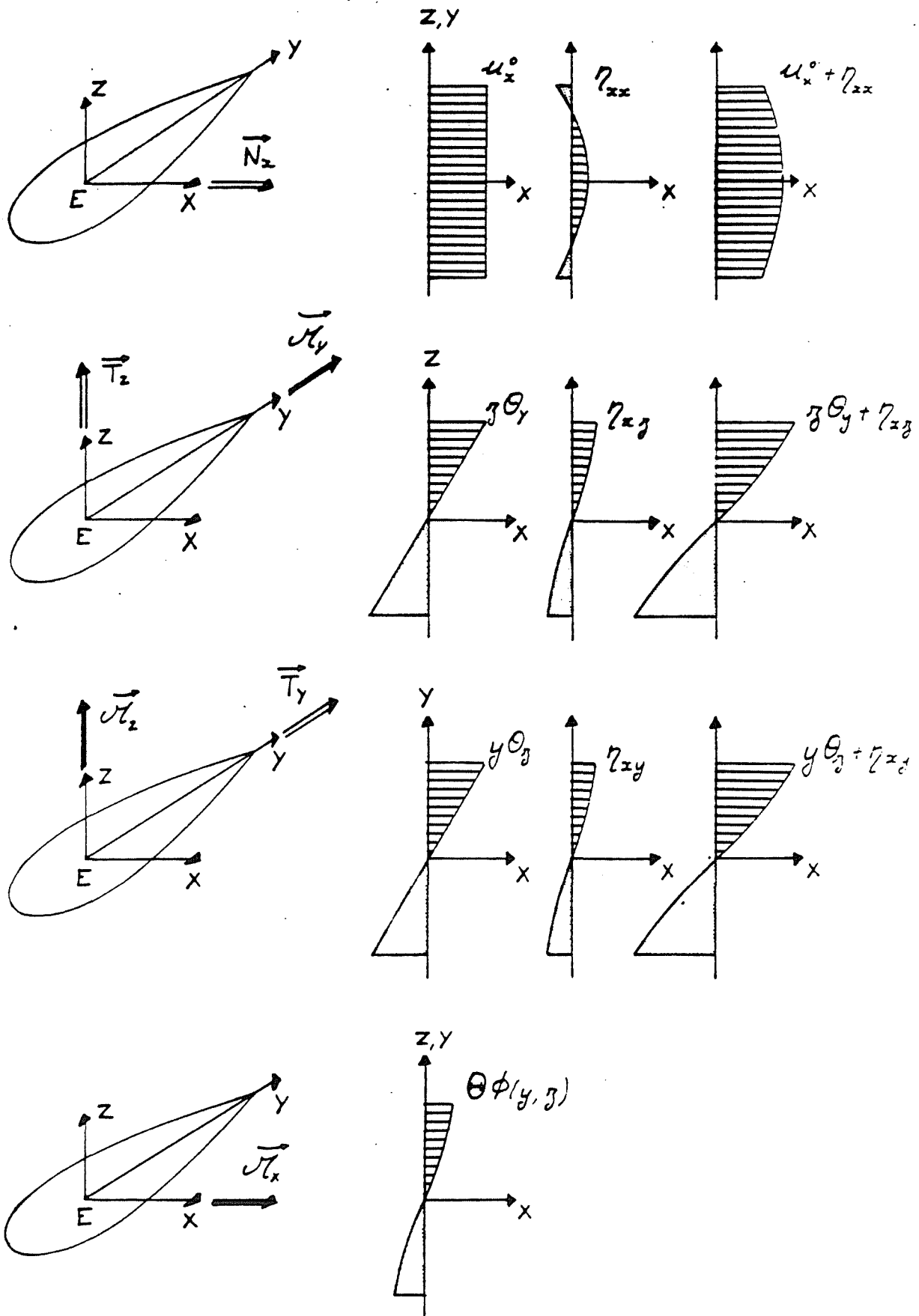
Figure 3 :   Normal and warping displacements of a section under normal forces, bending moments, shear forces and moment of torsion
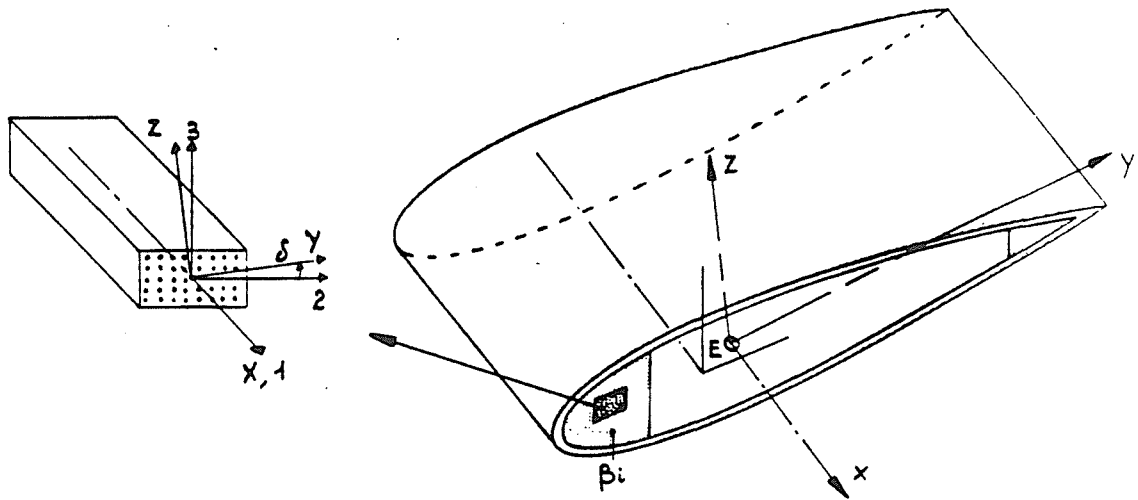
a) Rear and front spars composed of unidirectional fibres oriented along the X axis

b) Blade skin composed of composite laminate
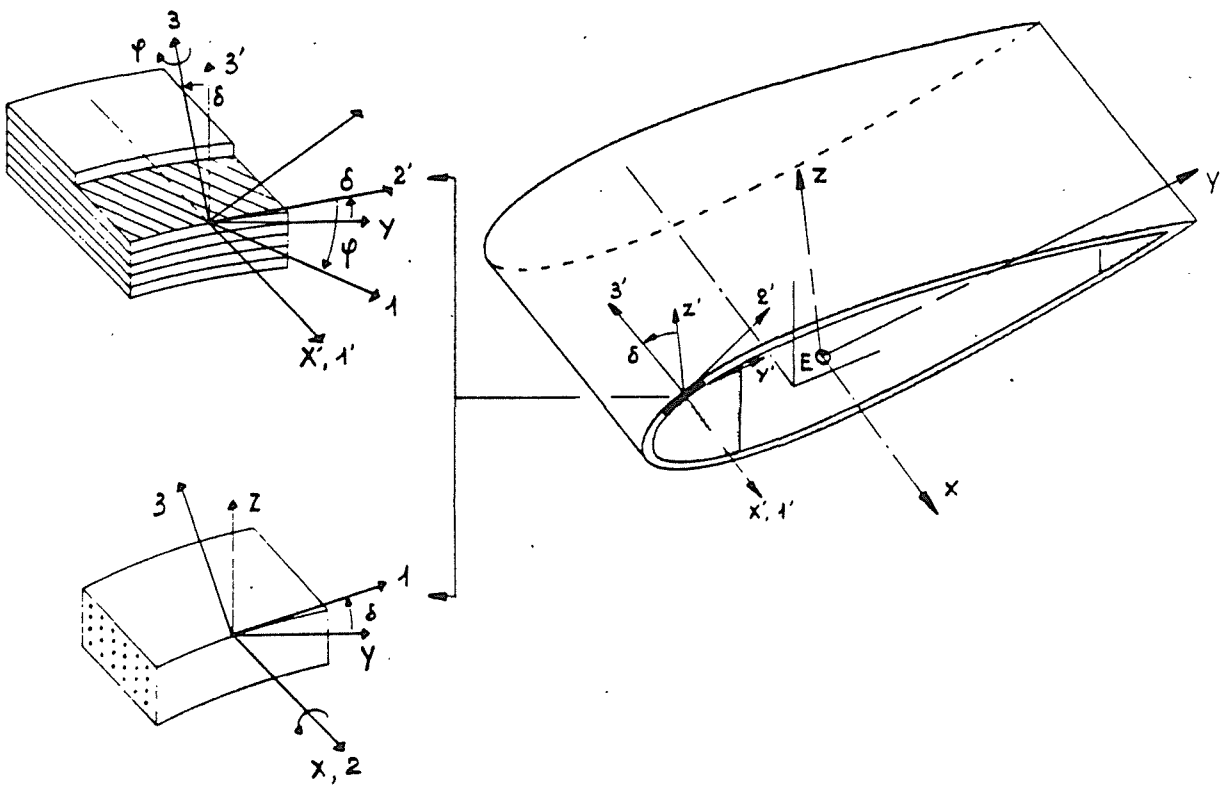
c) Blade skin composed of unidirectional composite

Figure 4 :   Three examples of composite material disposition inside the blades
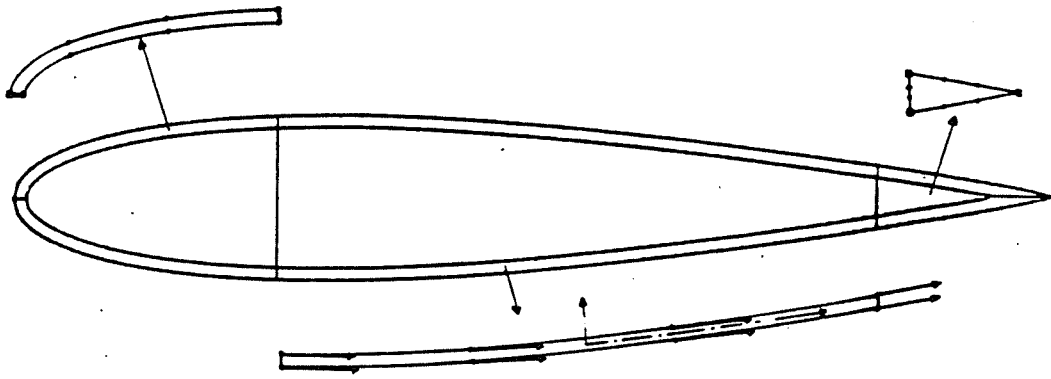
Figure 5 :   An example of sub-domain decomposition of a blade section
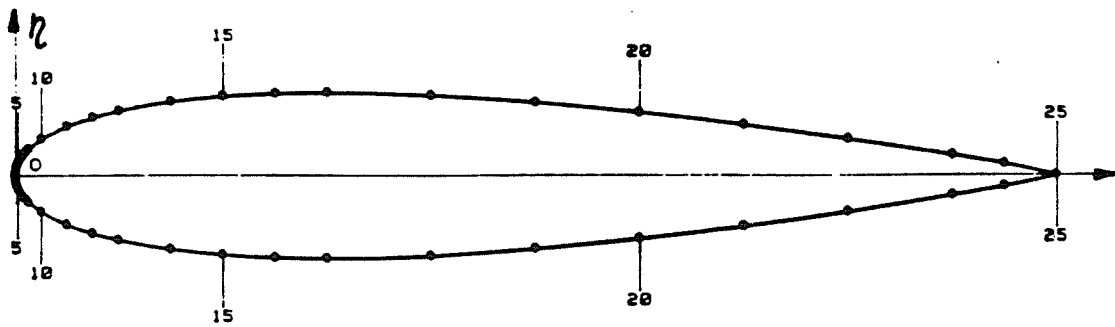
a)   Airfoil shape smoothing with cubic splines
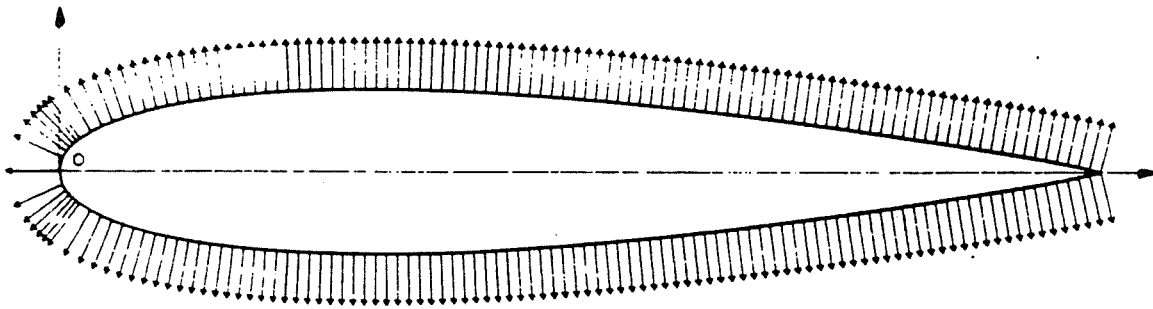
b)   Visualisation of the airfoil external unit normal vectors
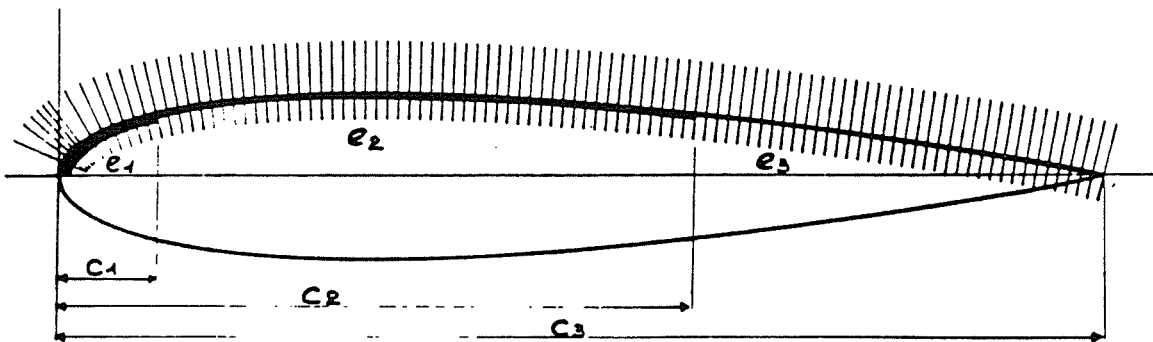
c)   Using of the unit normal vectors for the calculation of the composite layer thicknesses

Figure 6 :   Discretization method of a typical airfoil used in helicopter blade models
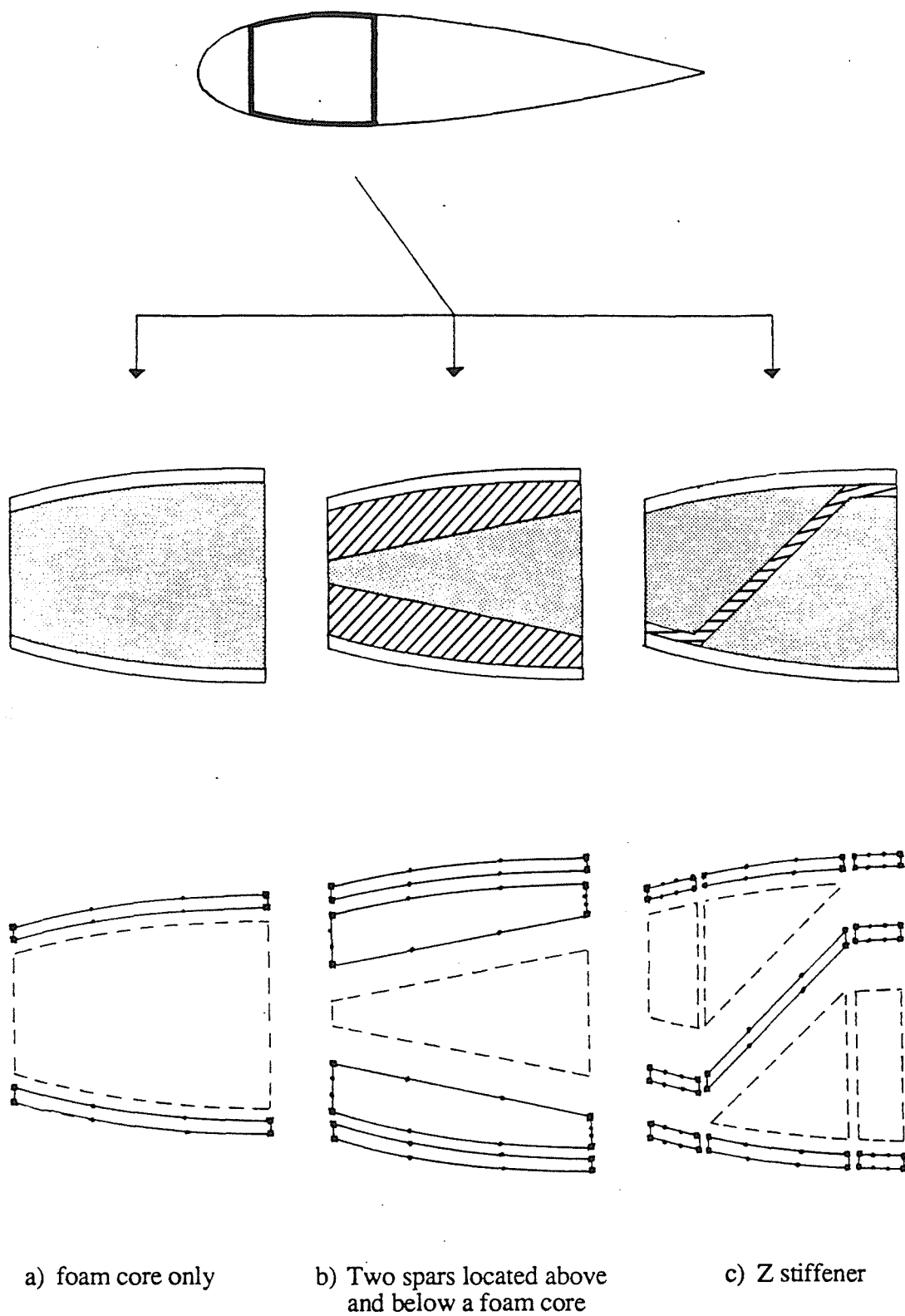
a) foam core only

b) Two spars located above and below a foam core

c) Z stiffener

Figure 7 :   Three examples of section discretization method into sub-domains
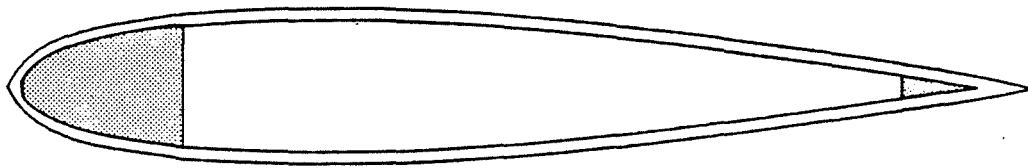
a)   Section geometry
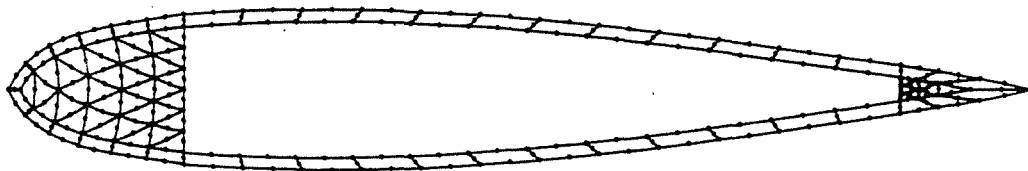
b)   Discretization of the section for the FEM
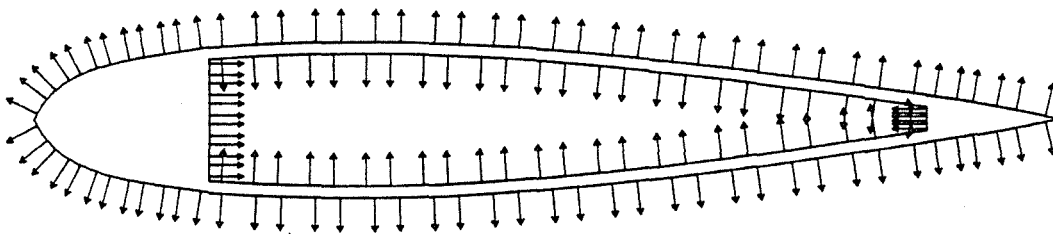
c)   Visualisation of the unit normal vectors along the free edges of the section, used
     in the calculation of equivalent surface forces deriving from the torsion boundary
     conditions
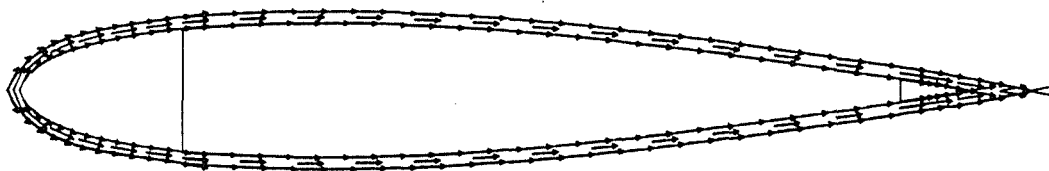
d)   Visualisation of the composite material fiber orientations calculated by the
     meshing program.
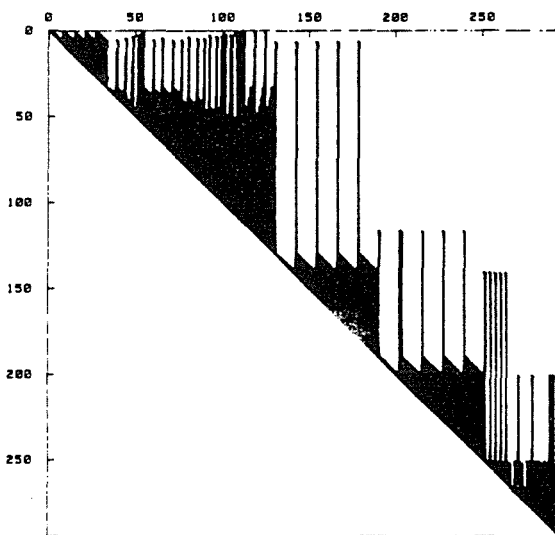
e) Skyline memory map of the global stiffness
   matrix before node renumbering
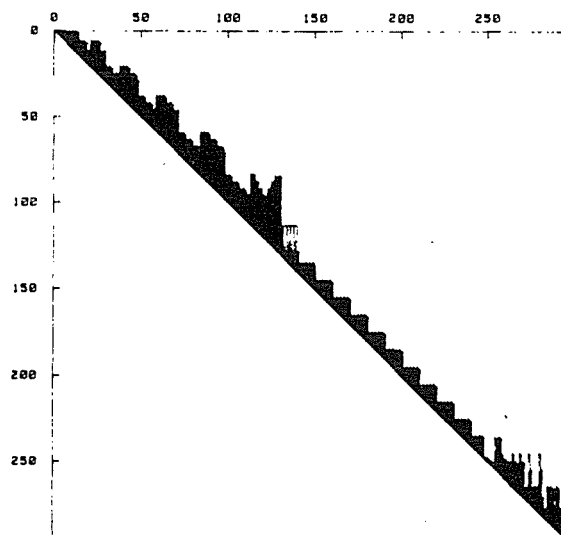
f) Skyline memory map of the global stiffness
   matrix after node renumbering

Figure 8 :   An example of the meshing method applied to a classical helicopter blade section
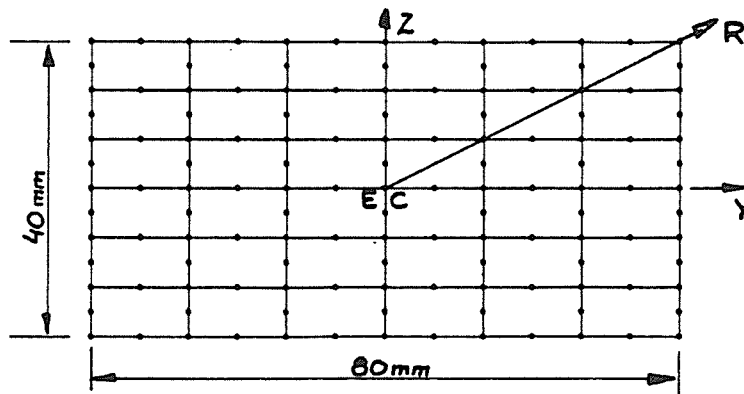
a) Discretization of the rectangular section for the FEM
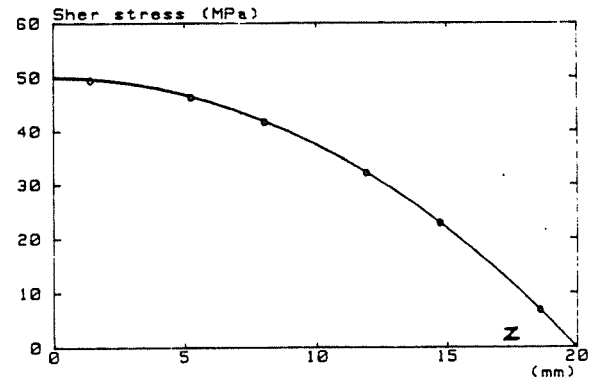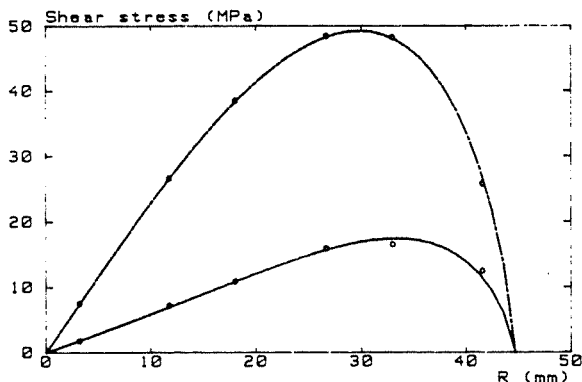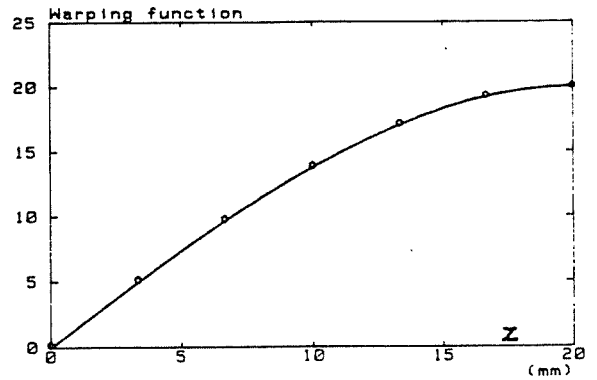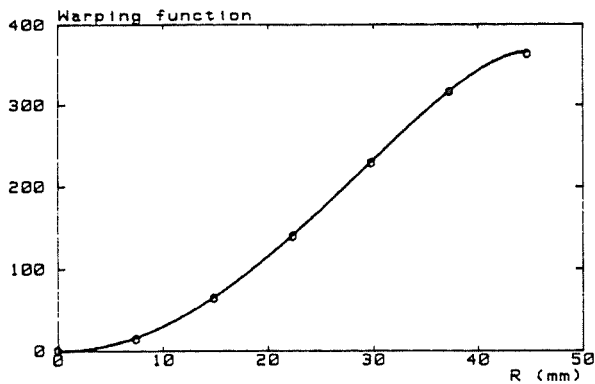
b) FEM values (o) and theoretical distributions of the torsional warping function ϕ and associated shear stresses σ_{xy} and σ_{xz}, vs. radial position R

c) FEM values (o) and theoretical distributions of the tranverse shear warping function g_o and associated shear stress σ_{xz}, vs. Z axis
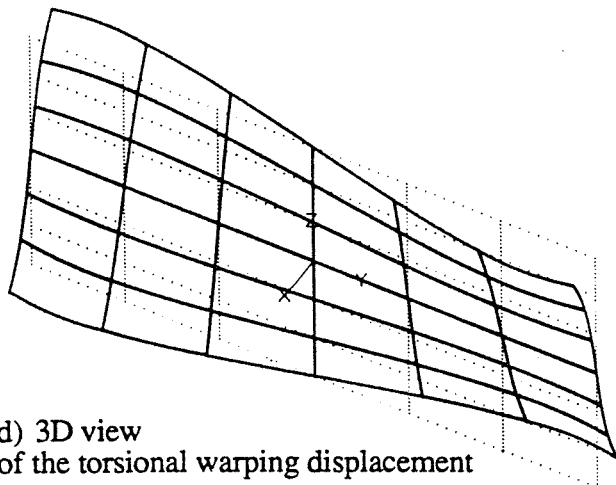
d) 3D view of the torsional warping displacement
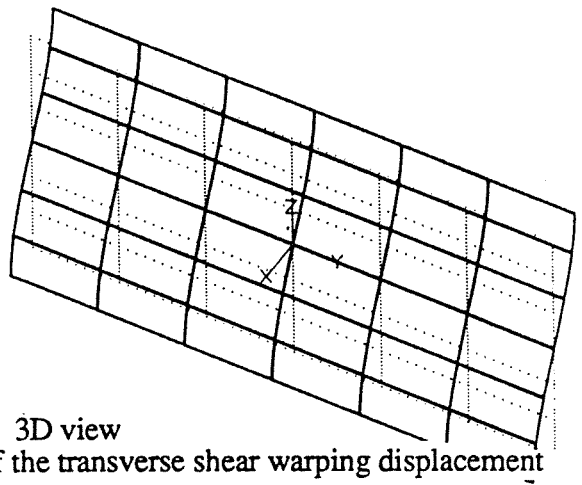
e) 3D view of the transverse shear warping displacement

Figure 9
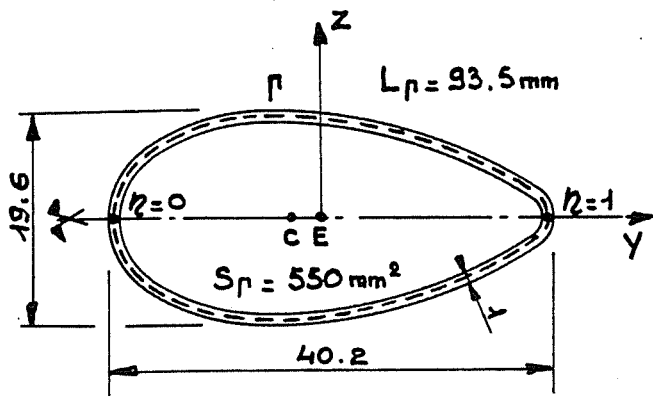
a) Dimensions of a simple airfoil
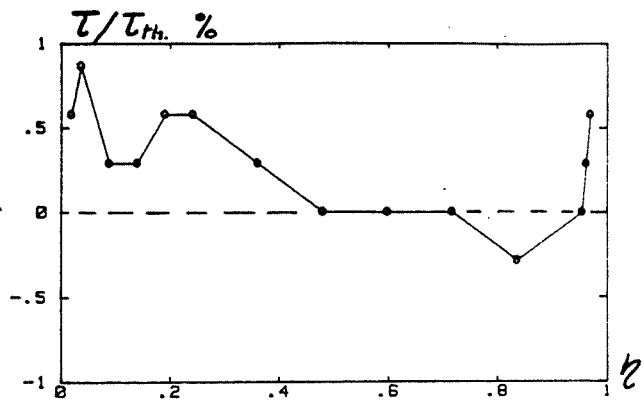
b) Error in the FEM resultant shear stress τ vs. the curvilinear axis η.
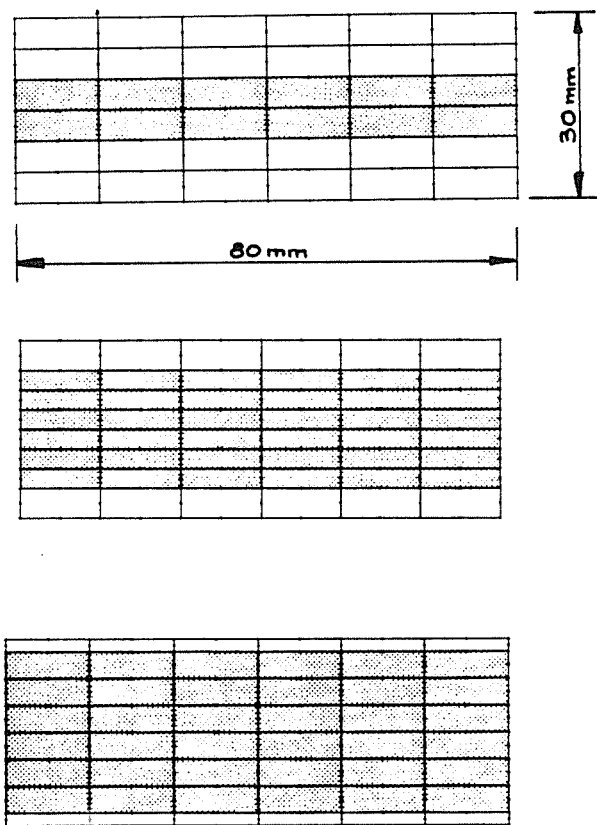
Figure 10

Figure 11:
Discretization of the sandwich sections with differents thickness ratios, used for the FEM calculation of the reduced section coefficient k_z
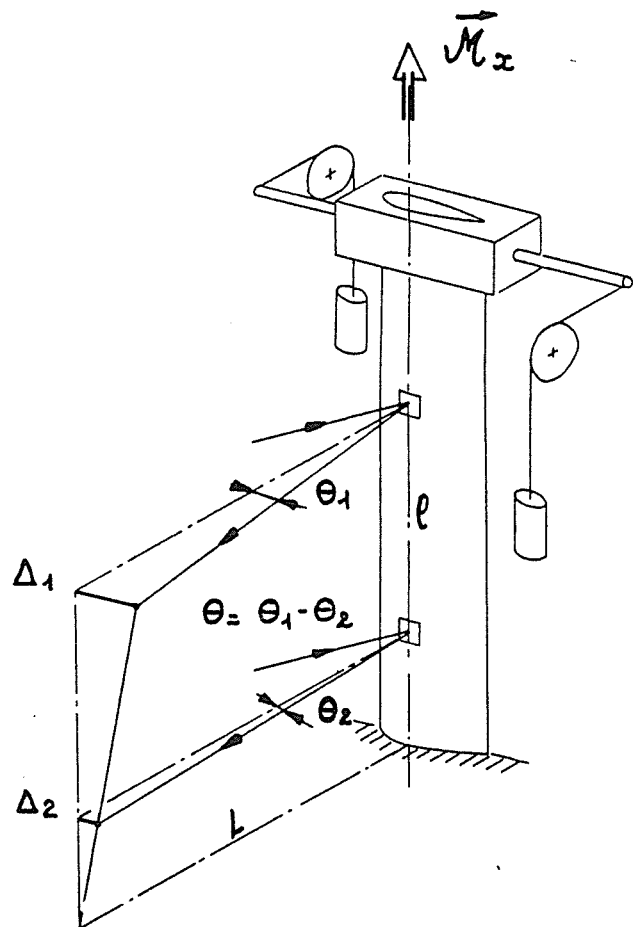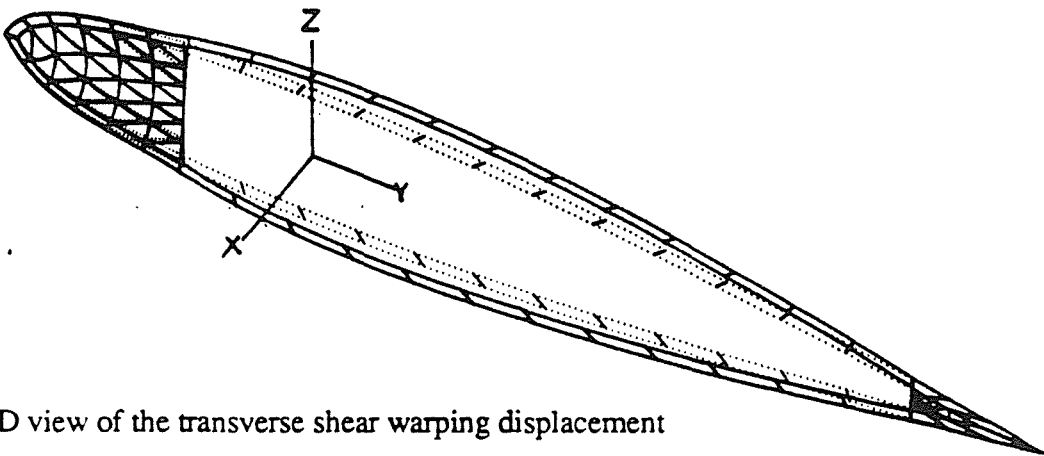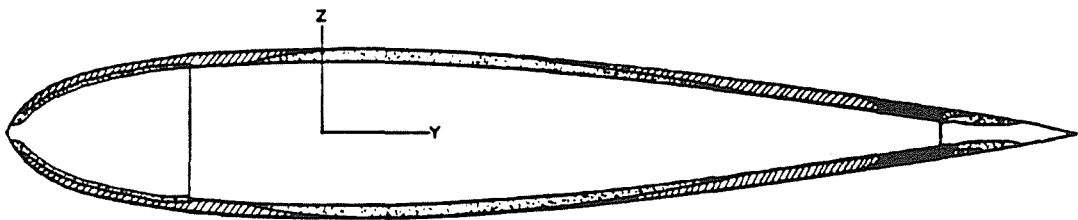
Figure 12 :
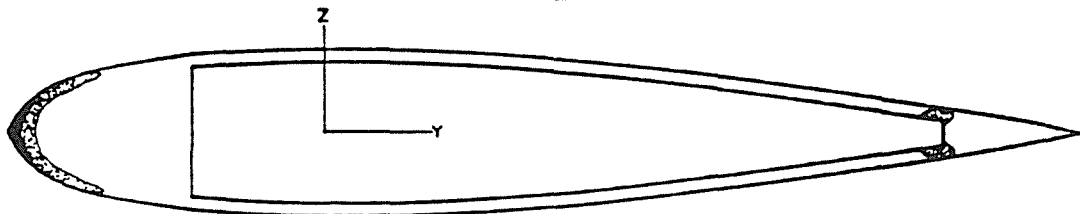Schematic view of the torsional stiffness measurement apparatus.
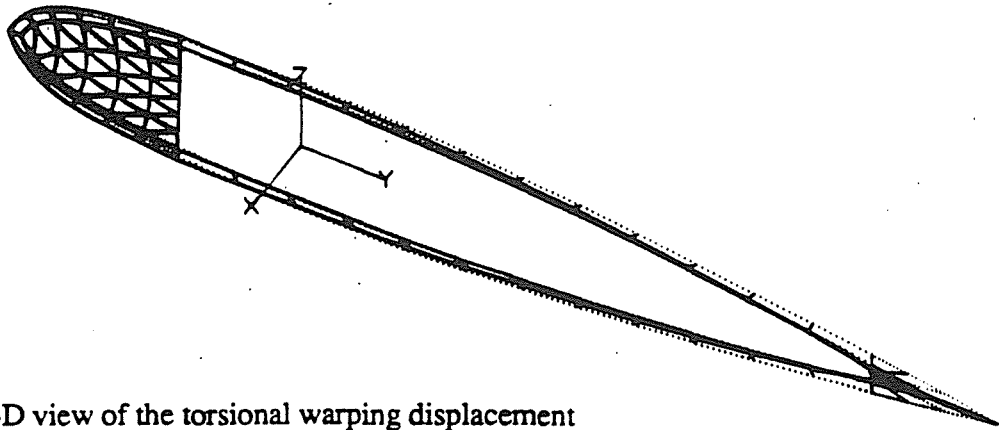
a) 3D view of the torsional warping displacement

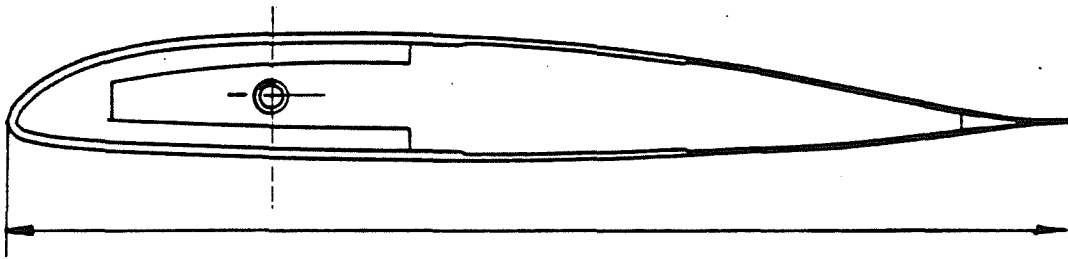b) 3D view of the transverse shear warping displacement

c) σ_{xy} shear stress distribution for the torsion

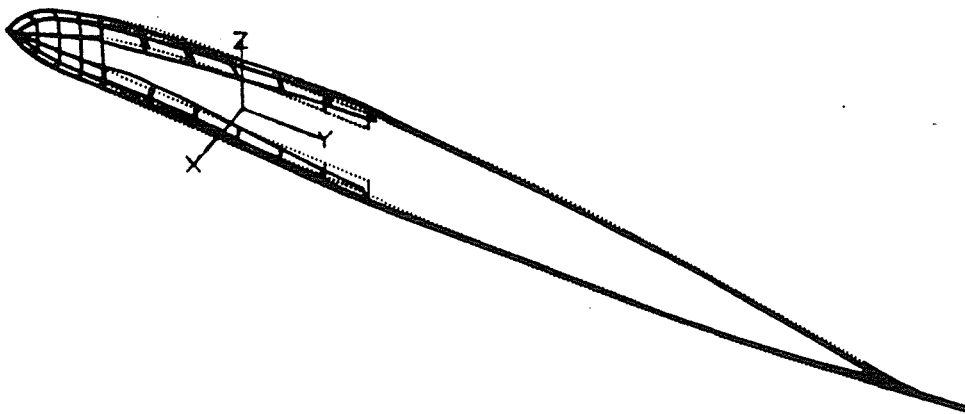|	0-10 MPa		10-20 MPa		20-30 MPa		30-40 MPa

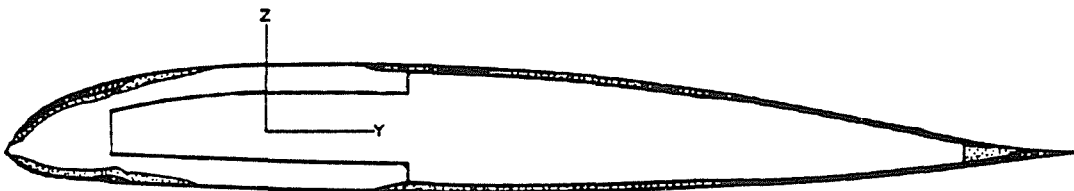d) σ_{xz} shear stress distribution for the torsion

Figure 13

a) Geometry of a realistic blade model section

b) 3D view of the torsional warping displacement

c) σ_{xy} shear stress distribution for the torsion

☐ 0-10 MPa   ▦ 10-20 MPa   ▨ 20-30 MPa   ■ 30-40 MPa

d) σ_{xz} shear stress distribution for the torsion

Figure 14